CA 27 4141
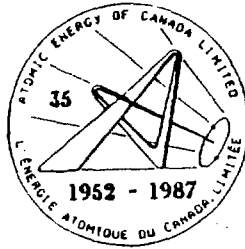
ATOMIC ENERGY
OF CANADA LIMITED

L'ÉNERGIE ATOMIQUE
DU CANADA LIMITÉE

COMPUTER SIMULATIONS OF CRYOGENIC
LINEAR ACCELERATOR STRUCTURES

SIMULATIONS PAR ORDINATEUR DES STRUCTURES
D'ACCÉLÉRATEURS LINÉAIRES CRYOGÉNIQUES

T. TRAN NGOC and J.-P. LABRIE

ATOMIC ENERGY OF CANADA LIMITED

COMPUTER SIMULATIONS OF CRYOGENIC LINEAR ACCELERATOR STRUCTURES

T. Tran Ngoc and J.-P. Labrie

Accelerator Physics Branch
Chalk River Nuclear Laboratories
Chalk River, Ontario KOJ 1J0

L'ÉNERGIE ATOMIQUE DU CANADA, LIMITÉE

SIMULATIONS PAR ORDINATEUR DES STRUCTURES
D'ACCÉLÉRATEURS LINÉAIRES CRYOGÉNIQUES

par

T. Tran Ngoc et J.-P. Labrie

RÉSUMÉ

Les structures d'accélérateurs linéaires cryogéniques ont un haut
rendement r.f. du fait de la résistivité réduite et de la haute capacité de
transfert thermique provenant du régime de transfert thermique sous
ébullition. On se sert d'une analyse de transfert thermique transitoire et
de contraintes thermiques par la méthode des éléments finis pour simuler le
comportement des structures d'accélérateurs linéaires au cours du
refroidissement brusque et prédire leurs caractéristiques au cours du
fonctionnement en (régime de) puissance.

COMPUTER SIMULATIONS OF CRYOGENIC LINEAR ACCELERATOR STRUCTURES

T. Tran Ngoc and J.-P. Labrie

Abstract

Cryogenic linear accelerator structures have high rf efficiency due to reduced resistivity and high heat transfer capability from the boiling heat transfer regime. Finite-element transient heat transfer and thermal stress analysis is used to simulate the behaviour of linear accelerator structures during quenching and predict their characteristics during power operation.

Accelerator Physics Branch
Chalk River Nuclear Laboratories
Chalk River, Ontario, Canada K0J 1J0

Nomenclature

R_s = surface resistivity

r = material resistivity

δ = skin depth

μ = material's permeability ($\mu_o = 4\pi \times 10^{-7}$ Ω-s/m)

f = frequency

ΔT = temperature change

α = thermal expansion coefficient

E = Young's modulus

σ = stress level

ν = Poisson's ratio

Δx = mesh size on finite element model

$\Delta \theta$ = time step increment for transient analysis

C, C_p = specific heat

ρ = density

k = thermal conductivity

Nu = Nussel's number = h D/k

Re = Reynold's number $(GD/v)^{0.8}$

Pr = Prandl's number = vCp/k

ρ_f, ρ_g = saturated liquid and vapor density respectively

h_{fg} = latent heat of vaporization

S = surface tension between saturated liquid and its vapor

g = acceleration of gravity

R = radius of a cylindrical structure

h = heat transfer film coefficient

D = cooling channel diameter

G = mass flow rate

v = dynamic viscosity

T_{Sat} = saturation temperature of the coolant

T_w = cavity wall temperature

T = temperature

L = Lorentz ratio

CHF = critical heat flux

1. INTRODUCTION

The rf efficiency of linear accelerator structures is determined by the ratio of beam power to total rf power, the beam loading coefficient. Improvements to the overall linac efficiency are obtained by minimizing the rf power losses in the cavities. However, in heavily beam loaded systems, improvements to linac efficiency become relatively small; the control and stability of linac operating characteristics at high power are usually of greater concern.

RF power losses at the surface of cavities are directly proportional to the material's surface resistivity given by

$$R_s = \frac{r}{\delta} \tag{1}$$

The skin depth, δ, is given by

$$\delta = (\frac{r}{\pi\mu f})^{1/2} \tag{2}$$

Wall losses are proportional to the cavity dimensions and hence, the rf efficiency of accelerator structures is increased by operating at higher frequencies with low resistivity materials.

Experimental data on the electrical resistivity of metals[1] show that

(i)   Metals have a resistivity in the range 1.5 to 150 $\mu\Omega$-cm at room temperature.

(ii) Their resistivity increases approximately linearly with temperature.

(iii) The total resistivity is composed of thermal, impurities and magnetic contributions with the thermal contribution decreasing at low temperature, roughly as the third to fifth power of temperature.

(iv) There is a relationship between the electrical resistivity and thermal conductivity of metals, called the Wiedemann-Franz-Lorentz law, namely[1]

$$kr = LT \tag{3}$$

where the Lorentz ratio, L, approaches 2.45×10^{-8} (volt/kelvin)^2 for pure metals at high and very low temperatures. At intermediate temperatures, the thermal conductivity usually increases less than the electrical conductivity and the Lorentz ratio can be some 70% lower[1].

Normal linear accelerator structures are usually made from Oxygen Free High Conductivity (OFHC) copper. Operating an OFHC copper structure at liquid nitrogen temperature reduces the material's surface resistivity[2] by about 66% and the power losses at the same energy gradient by a factor of about 3. Structures operated at liquid nitrogen temperature also have the high heat removal efficiency of the boiling heat transfer process[3].

Power dissipation in a cryogenic structure will be limited by thermal stresses in the cavities and by the critical heat flux of the cooling liquid. Thermal stresses may develop beyond the material yield point causing permanent detuning of the structure. Film boiling of the cryogenic coolant occurs beyond the critical heat flux, causing a temperature runaway of the structure.

This report describes the results of finite element computer modeling of the properties of coupled cavity linear accelerator structures operated in a pool of liquid nitrogen. Material properties at low temperature are reviewed and a time variation of the thermal stresses during cooldown is described. Approximations used to simplify the computer modeling are discussed and the simulations are applied to a 1300 MHz side-coupled structure.

2.   PROPERTIES OF MATERIALS AT LOW TEMPERATURE

Material properties vary significantly between room and cryogenic temperatures and these changes must be taken into consideration in the heat transfer and thermal stress analysis of cryogenic structures.

The experimental data for the most temperature sensitive material properties relevant to the analysis of accelerator structures operated at low temperature as well as the thermodynamic and heat transport properties of liquid nitrogen

and hydrogen are shown in Fig. 1 through 11. The data are taken from references 4, 5 and 6. The temperature dependence of the thermal expansion coefficient, thermal conductivity, heat capacity and electrical resistivity of OFHC copper and aluminum are shown in Figs. 1 to 4. Variations of the yield and tensile strength of annealed OFHC copper as a function of temperature are shown in Fig. 5. The saturated liquid density, thermal conductivity and viscosity of liquid nitrogen and hydrogen are given in Figs. 6 to 11.

3. ACCELERATOR STRUCTURE QUENCHING

At the beginning of the quenching process from room to cryogenic temperatures, the outer boundary surface of the accelerator structure is subjected to a step change in temperature and a thermal shock develops at the surface layer characterized by a sharp temperature gradient across a very small depth into the structure. The resulting stress intensity is the same everywhere at the outer boundary surface and is independent of the shape of the structure. The stress resulting from the initial thermal shock is given by

$$\sigma = \frac{\Delta T \ \alpha \ E}{1 - \nu} \tag{4}$$

The stress level at the boundary surface at the beginning of the quenching may cause surface yielding or cracking. The damage is however localized on a thin surface layer and will not affect the structure properties and hence can be tolerated.

The second stage of transient behaviour during cooldown depends on the structure shape and on the magnitude of the temperature change. Depending on the cooldown rate, the temperature distribution in the structure at a given time can lead to large stresses at discontinuities and stress concentration areas. The stress intensities can be calculated by transient heat transfer analysis analytically or numerically using a finite-difference or a finite-element method. In numerical analysis, care must be taken to avoid unstable

conditions yielding unrealistic results[7]. The stability criterion for a
forward finite-difference approximation of a two dimensional system during
cooldown is

$$\Delta\theta \geq \frac{1}{4} \frac{\Delta x^2 \, C\rho}{k} \tag{5}$$

Hence the smallest time step increment in an numerical analysis depends on the
largest mesh size used in the structure modeling.

The boundary conditions imposed in the analysis of a quenching problem are
quite complicated. When a structure is plunged in a pool of cryogenic liquid,
the structure's initial thermal mass boils the coolant off and the cooling
process is controlled by the structure's outer wall temperature. A typical
pool boiling curve is shown in Fig. 12. The boiling process could begin in
the film boiling regime, then evolve into the transition and nucleate boiling
state, and end in the liquid natural convection regime as the structure wall
temperature approaches that of the cooling fluid. Several empirical
expressions, each valid for one particular cooling regime, are required for
the analysis. Furthermore, the heat flux varies locally at the boundary
surface of the structure during quenching[8],[9]. However, to simplify the
analysis, a uniform and constant structure boundary temperature is usually
assumed. This assumption is valid for structures of small dimensions or with
high thermal diffusivity.

4. COMPUTER MODELING OF STRUCTURES OPERATED AT LOW TEMPERATURE

Steps required for the analysis of accelerator structure behaviour at cryo-
genic temperatures are essentially the same as those that were developed for
room temperature linac structures[10]:

(i)   The surface power density distribution in the cavities is calculated with SUPERFISH[11].

(ii) The heat load distribution, heat fluxes and heat transfer coefficients at the boundary surfaces are estimated.

(iii) A preliminary heat transfer analysis is made and the resulting calculated heat fluxes are compared with the initial estimates.

(iv) An iteration using step (ii) and (iii) is made to obtain good estimates of the heat flux distribution.

(v)   A thermal stress analysis is performed.

(vi) Changes in the accelerator structure rf parameters frequency shifts, changes in Q values, are obtained from the thermal deformations and the cavity temperature distribution.

The power handling capability of room temperature linear accelerator structures is usually limited by the material yield strength (69 MPa for annealed OFHC copper[2]). Measurements have shown that the changes in an accelerator structure's rf parameters become unpredictable when thermal stresses exceed the material yield strength and hence the device becomes useless for controlled particle acceleration[12].

The yield strength of OFHC copper increases insignificantly at low temperature, see Fig. 5. The material yield strength may still be the limiting factor to the power handling capability of a cryogenic structure but power operation is also limited by the coolant critical heat flux, the maximum heat flux before reaching the film boiling regime. In fact, the boiling process is controlled by the heat fluxes at the boundary surface. When these exceed their critical value, there is a rapid transition from nucleate to film boiling, see Fig. 12, accompanied by a large increase in cavity wall temperature that could detune the structure.

The simplest method for cooling a cryogenic structure is by immersion in a pool of liquid although cooling channels with internal flow would increase the cooling effectiveness. For single phase forced convection, the empirical

relationship between the Nusselt number, Nu, Reynolds number, Re, and Prandt number, Pr,

$$Nu = 0.023 \ Re^{0.8} \ Pr^{0.4} \qquad (6)$$

used for water is usually valid for cryogenic liquids[5]. Boiling heat transfer regime with heat transfer coefficients usually about one order of magnitude greater than single phase flow will maximize the power handling capability of accelerator structures[13].

Data related to boiling heat transfer regime in cryogenic fluids are summarized in references 4, 5 and 18. The pool boiling curve for liquid nitrogen is shown in Fig. 12. The transient and steady state characteristics of a particular system could be represented by the same boiling curve[14]. The critical heat flux, CHF, for an infinite horizontal flat plate is obtained from the following empirical relationship[15]

$$CHF_{Plate} = 0.131 \ \sqrt{\rho_g} \ h_{fg} \ [Sg(\rho_f - \rho_g)]^{1/4} \qquad (7)$$

This can be generalized for different shaped objects[16] and in particular, for a horizontal cylinder (such as an accelerator structure) the critical heat flux can be obtained from the following expression[17]

$$\frac{CHF}{CHF_{Plate}} = 0.890 + 2.27 \ exp \ (-3.44 \ \sqrt{R'}) \qquad (8)$$

for values of R', defined by

$$R' = R(g(\rho_f - \rho_g)/S)^{1/2},$$

greater than 0.15.

Data on forced convection boiling of cryogenic fluids is very limited but the empirical relationships developed for water are expected to be applicable[4],[19].

5.   ANALYSIS OF A 1300 MHz SIDE-COUPLED STRUCTURE

5.1   Cavity Description

Figure 13 gives the dimensions of the 1300 MHz side-coupled cavities developed for the Los Alamos free electron laser experiments[20]. Cavities are made from OFHC copper and cooled at their outer surface.

5.2   Structure Quenching

In quenching the accelerator directly from room temperature to liquid nitrogen temperature, the magnitude of the thermal shock that develops at the outer cavity surface corresponds to a stress intensity of about (eqn. 4) 550 MPa. Hence the estimated stress intensity in the surface boundary layer of the structure exceeds the tensile strength of annealed OFHC copper[2] (345 MPa at 77 K, the boiling temperature of liquid nitrogen).

An axisymmetric finite-element model of the 1300 MHz side-coupled accelerating cavity segments has been built for an analysis of the transient behaviour of the structure during cooldown. Thermal stresses are larger in the accelerating cavities than in side-coupling cavities because of their size and cross-sectional shape. Therefore, the computer modeling was applied to the accelerating cavities only.

The finite-element model of the 1300 MHz accelerating cavity segments, shown in Fig. 14, uses 46 elements and 67 nodes. Axisymmetric 4-node isoparametric quadrilateral elements with 1 and 2 degrees of freedom per node are used for the heat transfer and the thermal stress analysis respectively. Structure quenching in liquid nitrogen is simulated by imposing a uniform outer surface temperature boundary condition of 77.4 K at time $\theta=0$. The time step used for

the transient cooldown analysis with the computer code MARC[21] is $\Delta\theta = 0.8$ s which satisfies the stability criterion for the numerical analysis (eqn. 5).

Temperature dependent properties of annealed OFHC copper, given in Table I, are specified by a series of linear curves. The transient analysis stops when all nodal temperatures are below 100 K.

Table I

Temperature Dependent Properties of OFHC Copper

Temperature	Thermal Conductivity	Heat Capacity	Thermal Expansion Coefficient
(K)	(W/mm-K)	(J/g/K)	$(10^{-6}/K)$
77	0.50	0.195	7.83
100	0.44	0.255	10.5
140	0.40	0.315	13.0
200	0.40	0.360	15.2
300	0.39	0.385	16.8

The temperature history of a few selected model elements are shown in Fig. 15. As expected, the calculated cooldown rate decreases inversely with the radial location of the elements. The temperature difference between the beam aperture region of the cavity webs and the outer cavity surface reaches a maximum 1 to 3 seconds after the analysis begins and all nodal temperatures fall below 100 K after 23 seconds.

Figure 16 gives the history of the Von Mises stress intensities of selected model elements. The results for the transient thermal stress analysis indicate that a maximum stress of 270 MPa is attained at the intersection of the nose cone with the cavity web wall (element No. 11, Fig. 14) 2 seconds from the beginning of the analysis. Near the structure outer surfaces, stresses decay exponentially with time. Absolute values of the stress intensities have large uncertainties since the results, obtained from an elastic analysis become invalid when the stress levels exceed the yield strength of the cavity material (69 MPa for annealed OFHC copper[2]). The results indicate however that structure precooling is required to prevent permanent detuning.

If the cooldown process is such that the stress intensity does not exceed the material yield strength, the frequency shift from room to liquid nitrogen temperature, estimated from the thermal expansion coefficients given in Table I, is 3.8 MHz. The corresponding frequency shift obtained by using the low temperature cavity profile calculated with MARC as an input to SUPERFISH is 3.6 MHz. The small difference between the calculated frequency shifts comes from stopping the analysis with MARC when all nodal point temperatures are below 100 K.

5.3 Computer Simulation of High Power Operation

The critical heat flux for liquid nitrogen is about 13 W/cm^2 (see Fig. 12). This will be attained at a power dissipation of about 75 kW/m in a 1300 MHz cavity.

Scaling the results from measurements of the power handling capability of room temperature OFHC copper structures without web cooling[12] indicates that the material yield strength would be reached at a power level of about 24 kW/m at room temperature in the 1300 MHz cavities.

The thermal expansion coefficient of OFHC copper decreases by a factor of about 2.1 at liquid nitrogen temperature (see Fig. 1), its thermal conductivity increases by a factor of about 1.5 (see Fig. 2) and its yield strength remains about the same. Hence, neglecting changes in low temperature material properties during power operation, thermal stresses in the cavity webs will exceed the yield strength of OFHC copper when operated in liquid nitrogen at power levels exceeding 79 kW/m. Limits on power dissipation imposed by the material's yield strength and the critical heat flux of liquid nitrogen are similar for the 1300 MHz structure.

A finite-element heat transfer and thermal stress analysis of the structure operating in the boiling heat transfer regime in a pool of liquid nitrogen has been made with the computed code MARC. At a reference power level of 10 kW/m, the corresponding heat flux at the outer surface of the cavities is

about 1.7 W/cm , the wall superheat, T_w-T_{Sat}, is 4.4 K and the cavity wall temperature is 82 K (see Fig. 12). The temperature and stress distributions are shown in Figs. 17 and 18. The maximum Von Mises stress is 11.5 MPa, located in the region of the cavity beam aperture (element #4, Fig. 14).

The calculated maximum Von Mises stresses are shown in Fig. 19 as a function of the dissipated power in the structure. The stresses vary non-linearly with power because of the variations of material properties with temperatures (see Figs. 1 to 3 and Table I). Thermal stresses reach the yield strength of OFHC copper when the 1300 MHz side-coupled structure is operated in a pool of liquid nitrogen at a power level of about 50 kW/m. This is in good agreement with the scaling of the power handling capability described above. Thermal stresses exceed the material yield strength at a dissipated power level about 2 times greater than at room temperature. Thermal stresses rather than the critical heat flux of liquid nitrogen limit the structure power handling capability.

Calculated frequency shifts and the relative changes in average surface resistivity are shown in Fig. 20 as a function of the power dissipated in the structure. Deformation in the low temperature cavity profiles calculated with MARC are used as an input to SUPERFISH to obtain frequency shifts as a function of power. Calculated frequency shifts for power operation in a pool of liquid nitrogen are about 2 times smaller than for room temperature operation because of the difference in thermal expansion coefficient of OFHC copper (see Table I).

Cavity surface temperature distributions are used to determine changes in the surface resistivity of the OFHC copper cavities as a function of power. At a power level of 50 kW/m, with thermal stresses reaching the material yield strength, the cavity surface resistivity is about 50% lower than at room temperature and hence, the effective shunt impedance and Q are about 2 times greater. Hence the structure can be operated in liquid nitrogen at average energy gradients about 2 times greater than at room temperature (the power

dissipated can be 2 times larger and the effective shunt impedance at the maximum power level is 2 times greater).

6. SUMMARY

This report discusses the methods and assumptions used for simulating the thermal behaviour of cryogenic linear accelerator structures during quenching from room temperature and steady state power operation. The analysis is applied to predict the behaviour of a 1300 MHz side-coupled structure cooled by immersion in a pool of liquid nitrogen.

Results indicate that:

- Precooling is required for bringing the structure from room to cryogenic temperature to prevent permanent detuning.

- Thermal stresses in the structure reach the yield strength of OFHC copper at a power level of 50 kW/m. This is about two times greater than at room temperature.

- Scaling of measurements of the power handling capability of room temperature coupled cavity linear accelerator structures is in good agreement with the results from the finite-element thermal stress analysis of cryogenic structures.

- The resistivity of OFHC copper is decreased by about 66% at liquid nitrogen temperature and hence, rf power requirements at a same energy gradient are reduced by a factor of about 3.

- The maximum average energy gradient can be made two times larger at cryogenic temperature.

REFERENCES

1. G.T. Meaden, "Electrical Resistance of Metals", Plenum Press, New York (1965).

2. OFHC Branch Copper, AMCO Sales, Library of Congress Catalog Card No. 62-11986 (1961).

3. T. Tran Ngoc and J.-P. Labrie, "Heat Transfer and Thermal Stress Analysis of RF Structures Operated in the Boiling Regime", Proc. of the 1987 Particle Accelerator Conf., Washington, DC (1987).

4. G.G. Halsenden, "Cryogenics Fundamentals", Academic Press (1971).

5. W. Frost, "Heat Transfer at Low Temperature", Plenum Press, New York (1975).

6. AMAX Copper Inc., "A survey of Properties and Applications – OFHC Branch Copper", AMAX Inc. (1974).

7. F. Kreith, "Principles of Heat Transfer", 3rd edition, Intext Press Inc. (1973).

8. J. Thibault and T.W. Hoffman, "Local Boiling Heat Flux Density Around a Horizontal Cylinder", Proc. 6th Int. Heat Transfer Conf., Toronto, 199 (1978).

9. S. Subramanian and L.C. Witte, "Quenching of a Hollow Sphere", J. of Heat Transfer, Transaction of the ASME, 109 (1987).

10. J. McKeown and J.-P. Labrie, "Heat Transfer, Stress Analysis and the Dynamic Behaviour of High Power RF Structures", IEEE Trans. Nucl. Sci., NS-30 (4), 3593 (1983).

11. K.H. Halbach and R.F. Holsinger, "SUPERFISH – A Computer Program for Evaluation of RF Cavities with Cylindrical Symmetry", Particle Accelerators $\underline{7}$, 213 (1976).

12. J.-P. Labrie and H. Euteneuer, "Power Handling Capability of Water Cooled CW Linac Structures", Nucl. Instr. and Meth. $\underline{A247}$, 281 (1986).

13. T. Tran Ngoc and J.-P. Labrie, "Boiling Heat Transfer Process in the Design of High Power Linac Structures", Proc. of the 1986 Linear Accelerator Conf., SLAC-303, 90 (1986).

14. D.R. Veres and L.W. Florschuetz, "A Comparison of Transient and Steady State Pool Boiling Data Obtained Using the Same Heating Surface", J. Heat Transfer, Trans. ASME, Series C, $\underline{93}$, 229 (1971).

15. N. Zuber, M. Tribus and J.W. Westwater, "The Hydrodynamic Crisis in Pool Boiling of Saturated and Supercooled Liquids", Int. Dev. in Heat Transfer, ASME, New York, 230 (1963).

16. J.S. Ded and J.H. Lienhard, "The Peak Pool Boiling Heat Flux from a Sphere", A.I.Ch.E. J., $\underline{18}$ No. 2, 337 (1972).

17. K.H. Sun and J.H. Lienhard, "The Peak Pool Boiling Flux on Horizontal Cylinders, Int. J. Heat Mass Transfer, $\underline{13}$, 1425 (1970).

18. H.Jr. Merte and J.A. Clark, "Boiling Heat Transfer with Cryogenic Fluids at Standard, Fractional and Near-Zero Gravity", J. Heat Transfer, Trans. of the ASME, Ser. C, $\underline{86}$, 351 (1964).

19. P.S. Shen and Y.W. Jao, "Non Equilibrium Phenomena in Cryogenic Two Phase Flow", Advanced Cryogenic Engineering, 17 (1970).

20. W.E. Stein, R.W. Warren, J.G. Winston, J.S. Fraser and L.M. Young, "The Accelerator for the Los Alamos Free-Electron Laser", IEEE J. of Quantum Electronics, QE-21, No. 7, 889 (1985).

21. MARC, Marc Analysis Research Corporation, 260 Sheridan Ave., Palo Alto, CA 94306, USA.
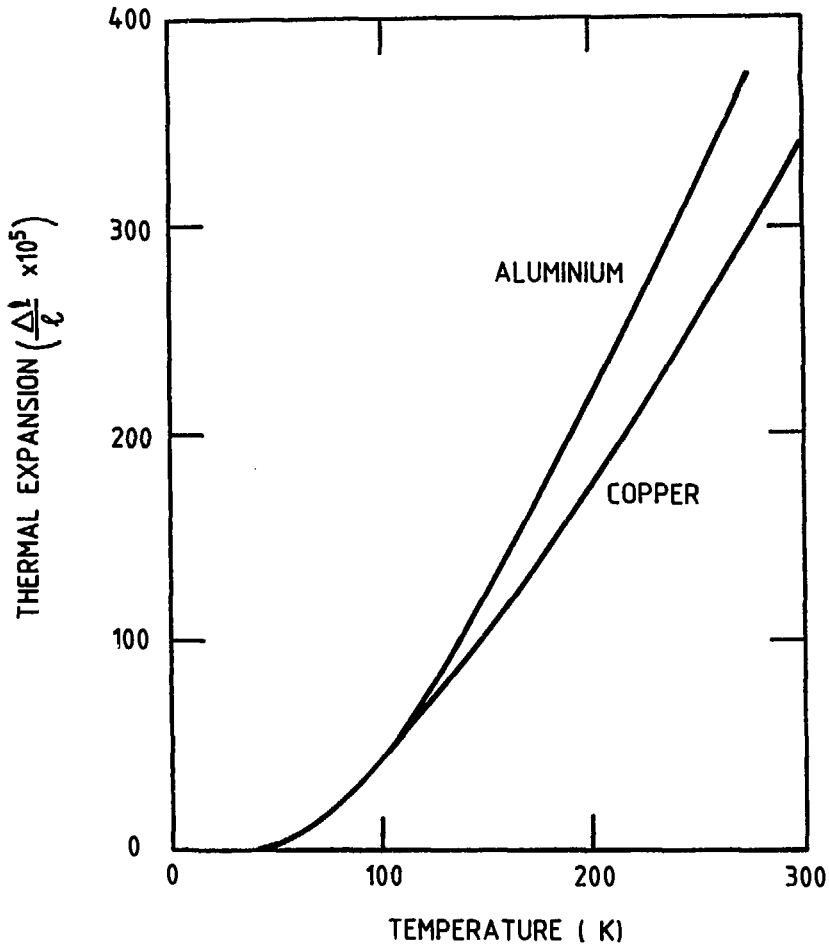
Fig. 1   Thermal expansion of aluminum and copper.
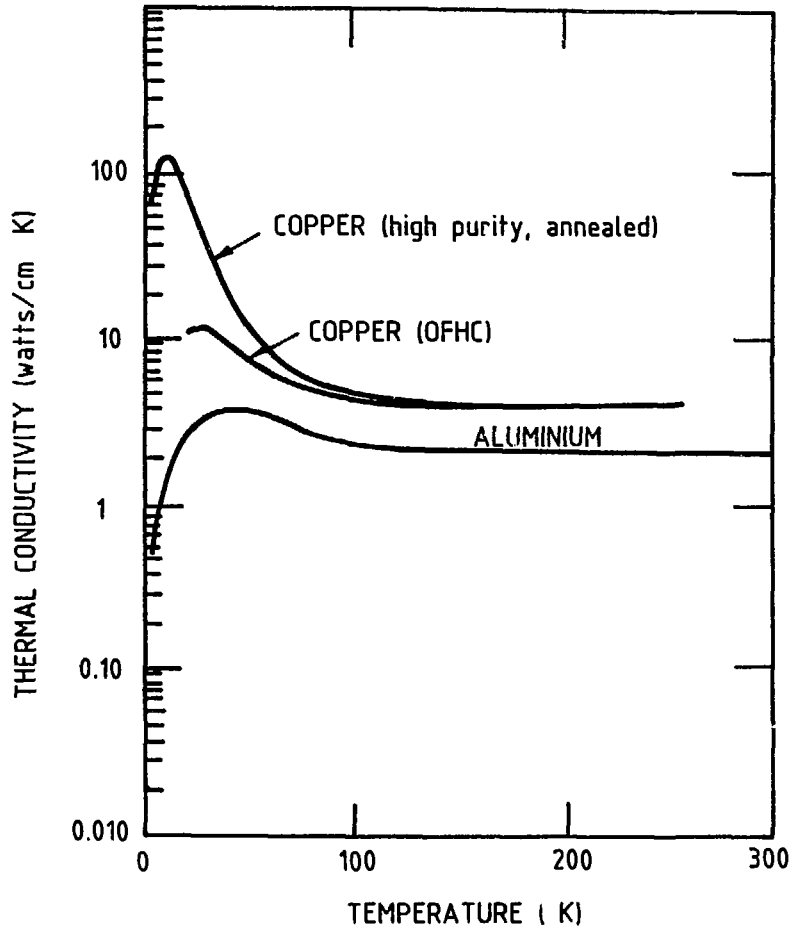
Fig. 2   Thermal conductivity of aluminum and copper.

15
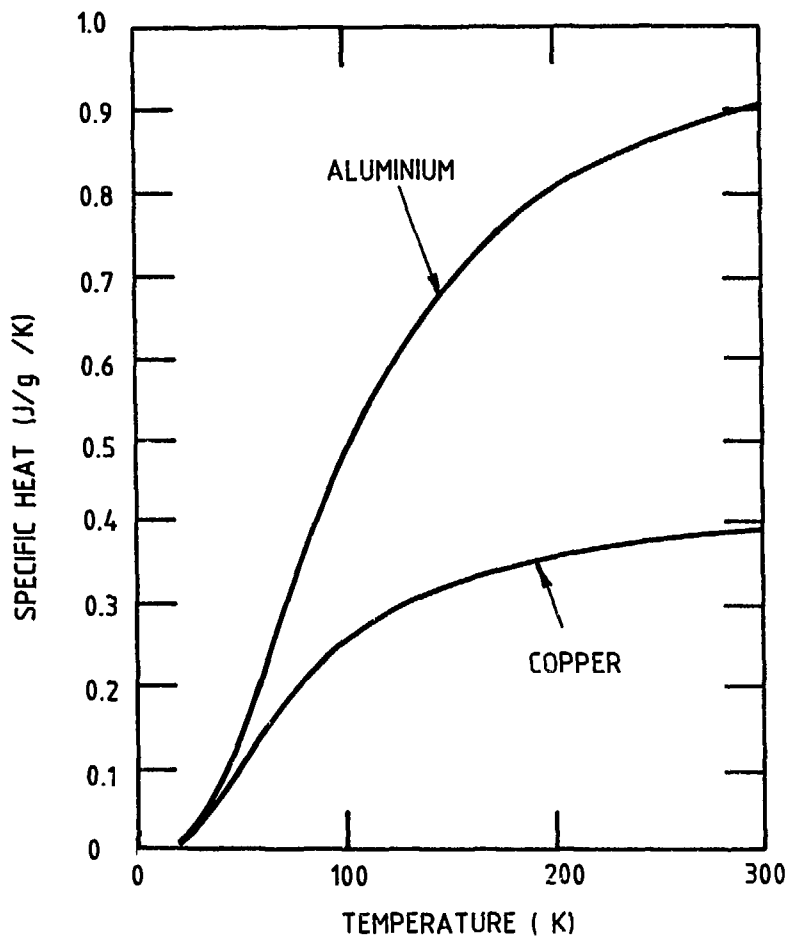
Fig. 3   Specific heat of aluminum and copper.
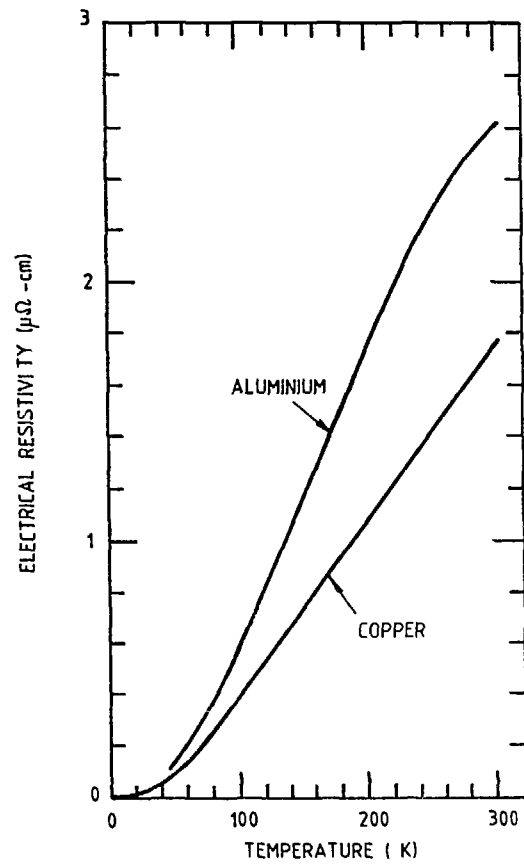
Fig. 4   Electrical resistivity of aluminum and copper.

16
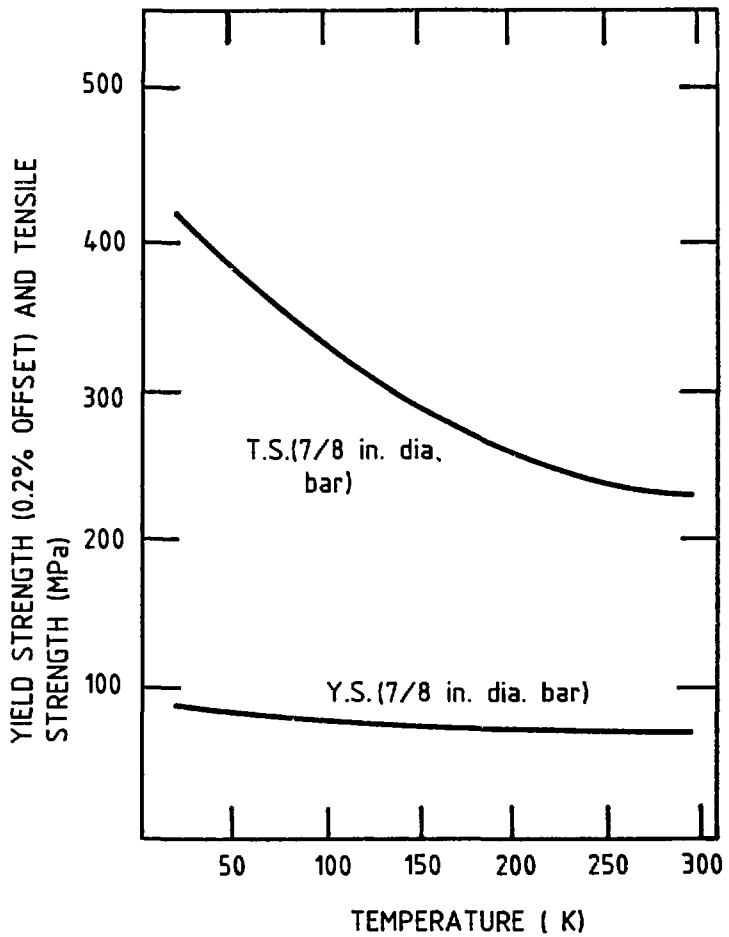
Fig. 5   Tensile and yield strength of OFHC copper.
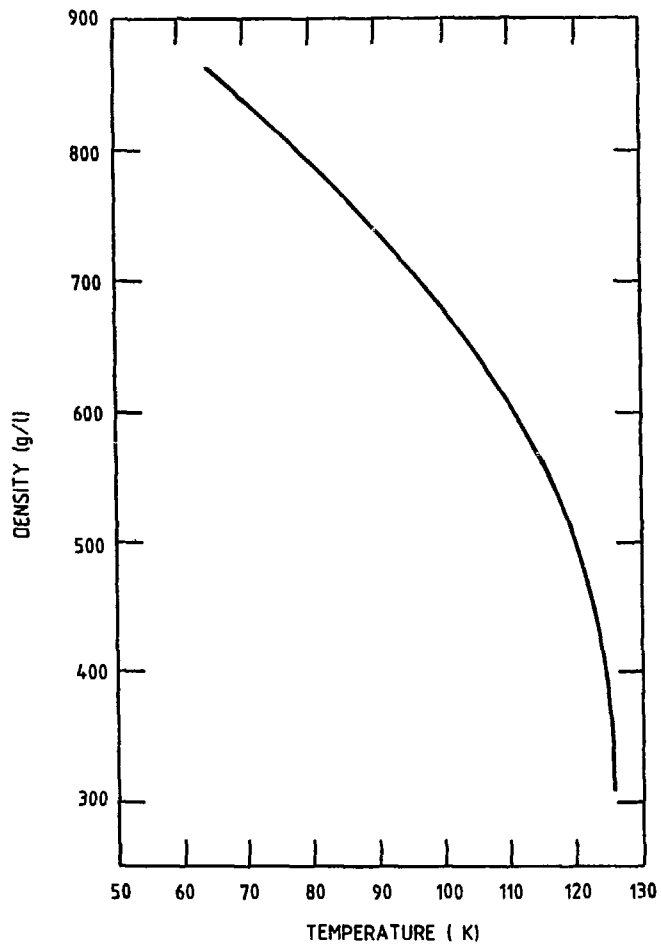
Fig. 6   Saturated liquid density of nitrogen.   Fig. 7   Saturated liquid density of normal-hydrogen.
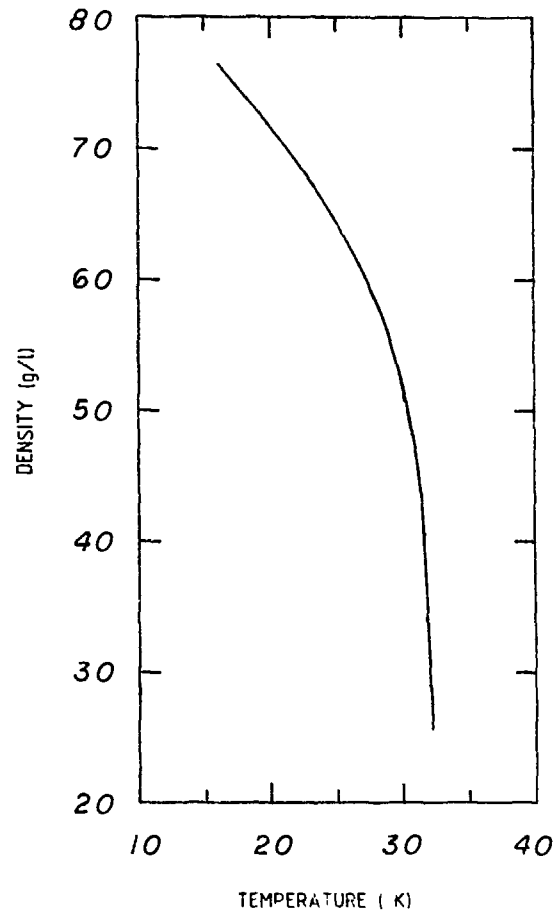
18
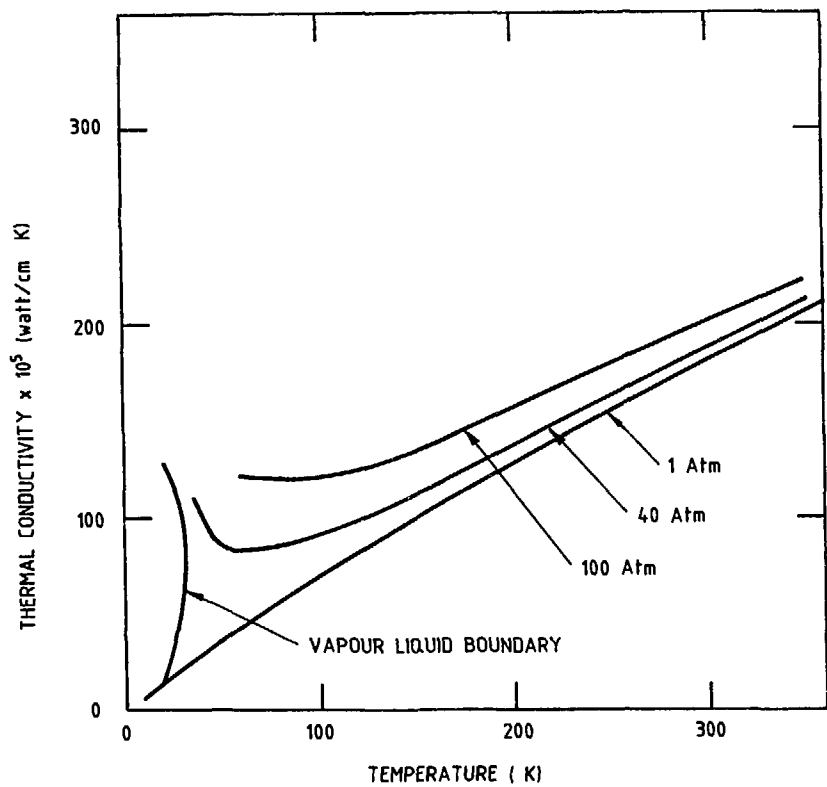
Fig. 8   Thermal conductivity of normal-hydrogen.
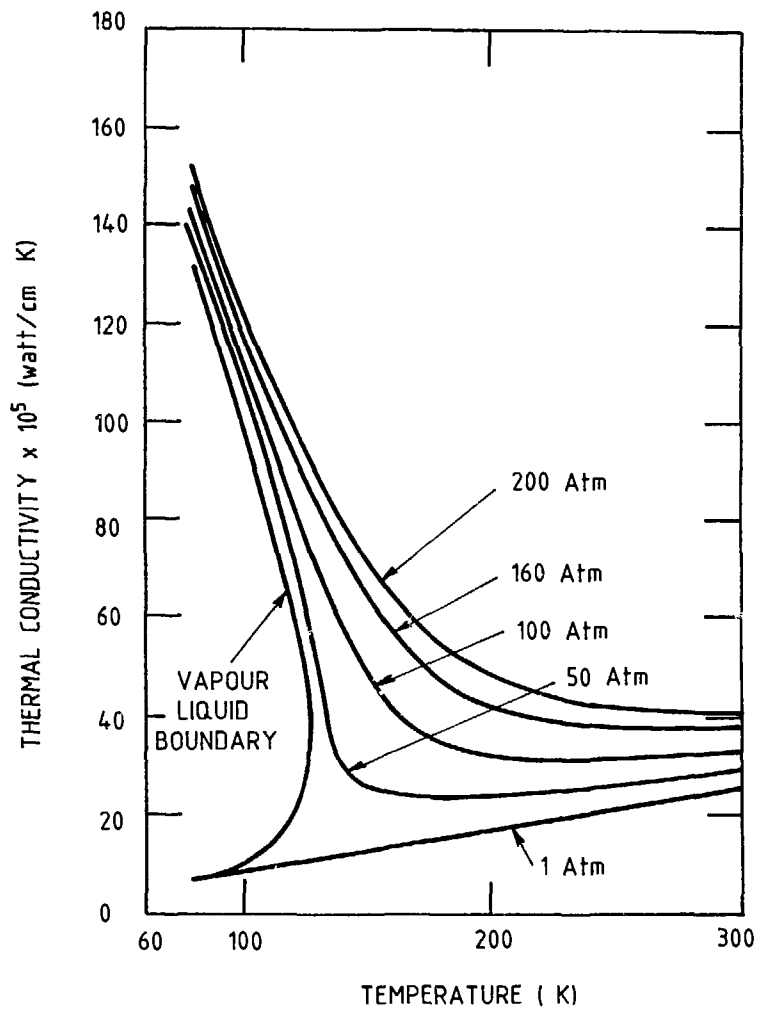
Fig. 9   Thermal conductivity of nitrogen.
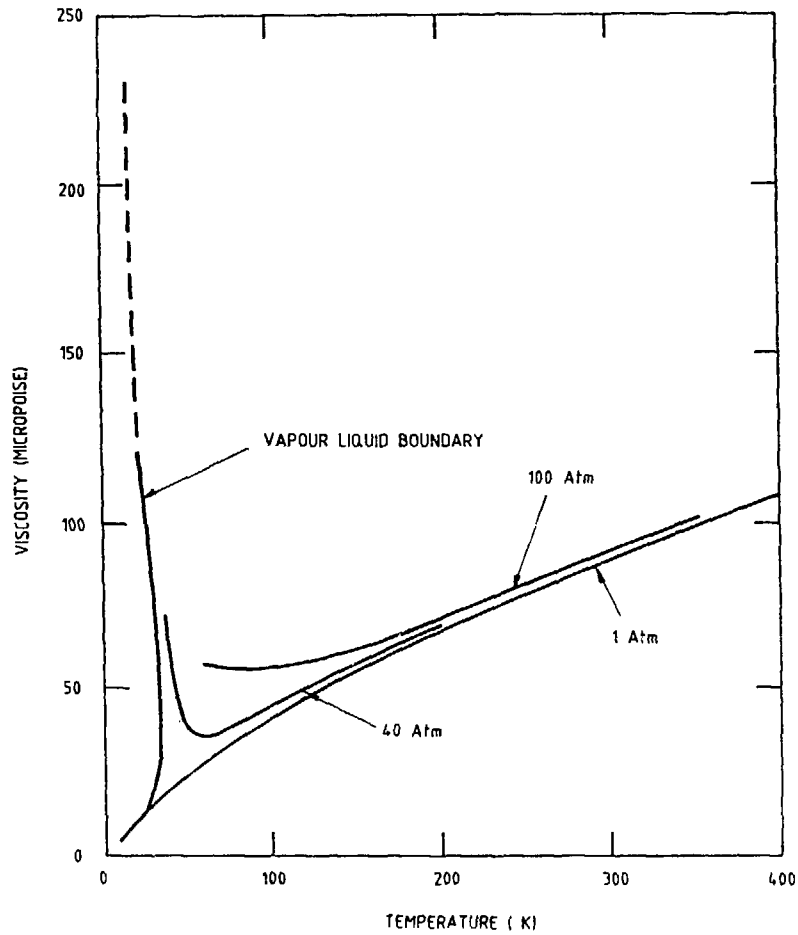
Fig. 10   Viscosity of normal-hydrogen.
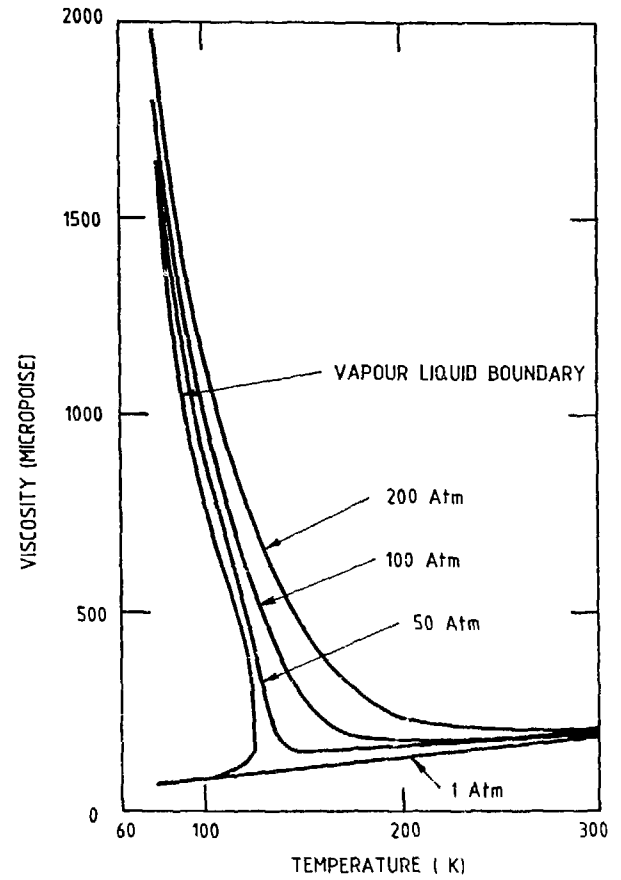
Fig. 11   Viscosity of nitrogen.
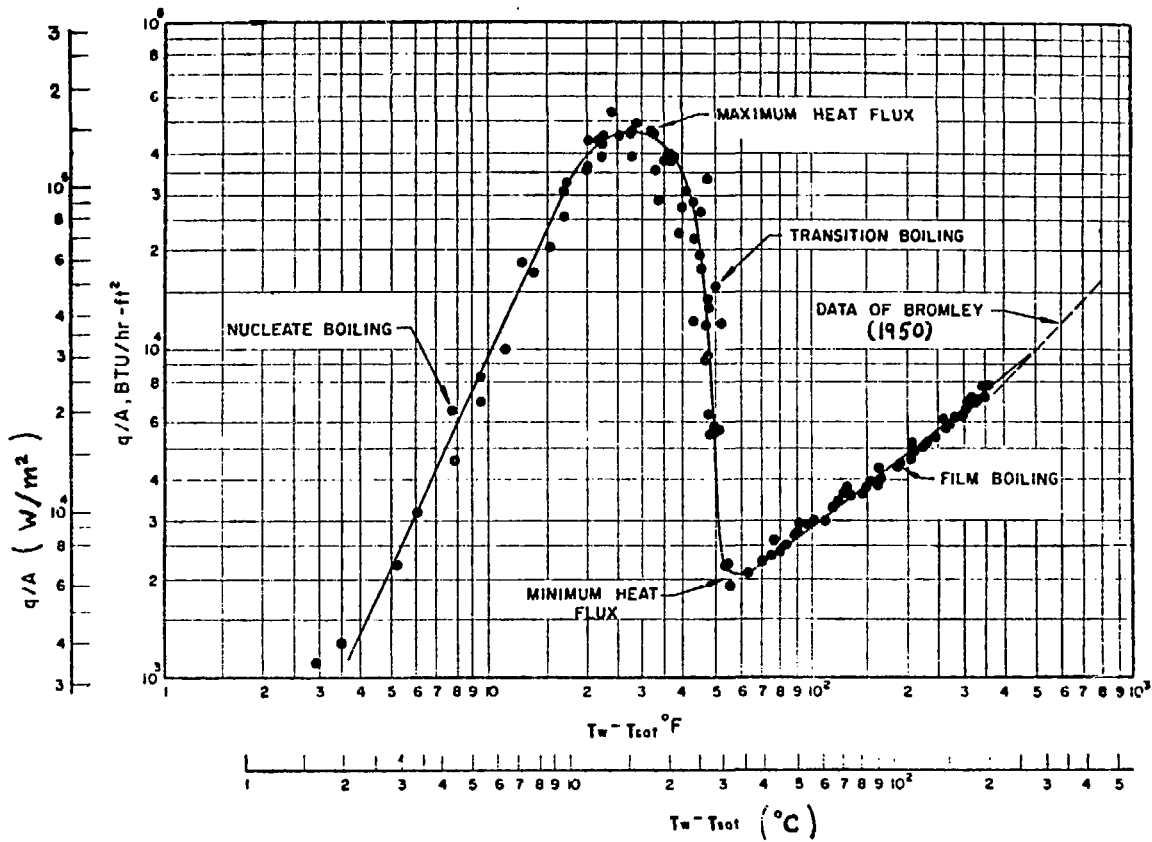
Fig. 12 Nitrogen pool boiling curve.

COUPLING CAVITY

COUPLING SLOT

ACCELERATING CAVITY
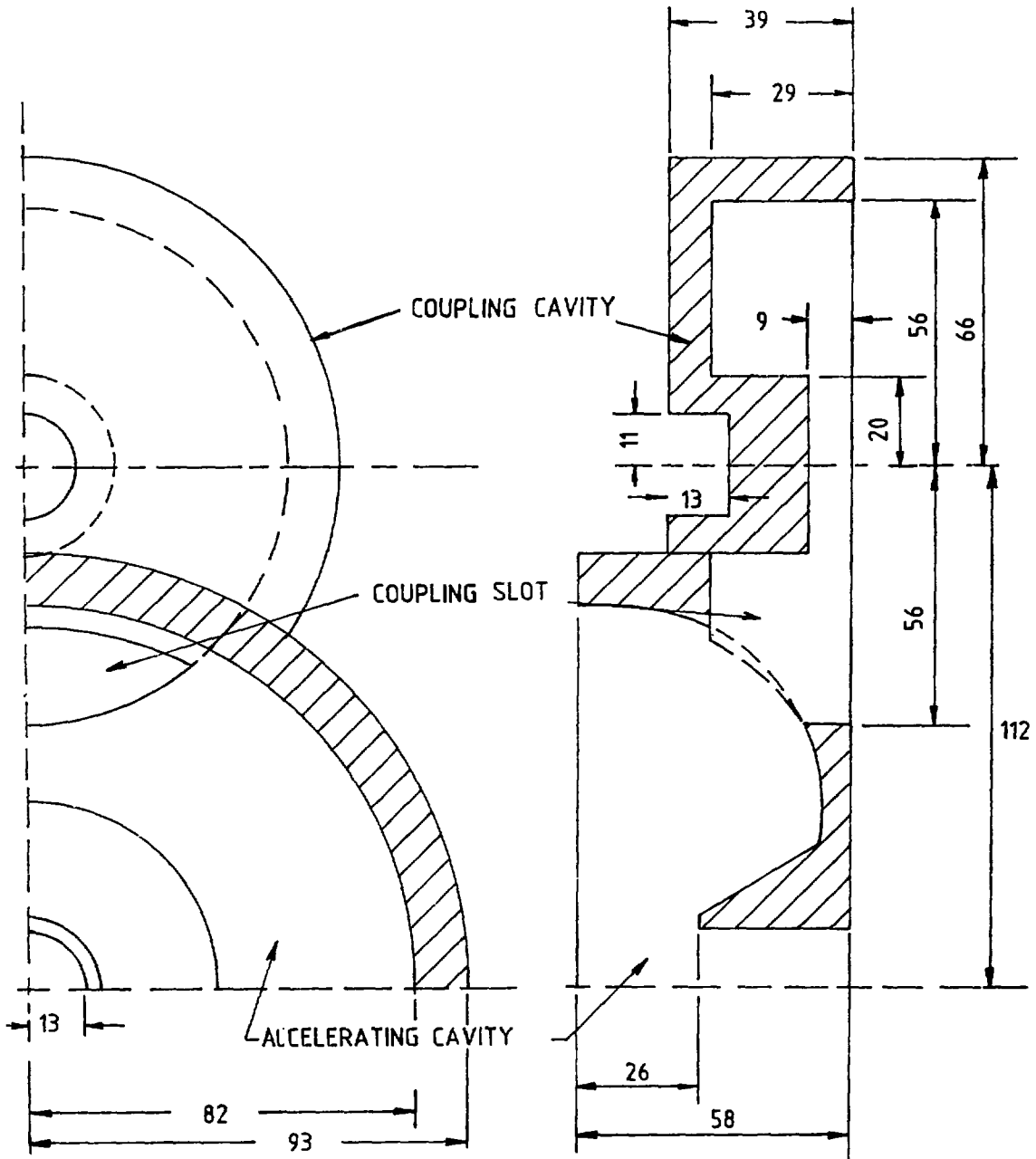
DIMENSIONS IN mm

Fig. 13 Dimensions in mm of 1300 MHz side-coupled cavity segment.
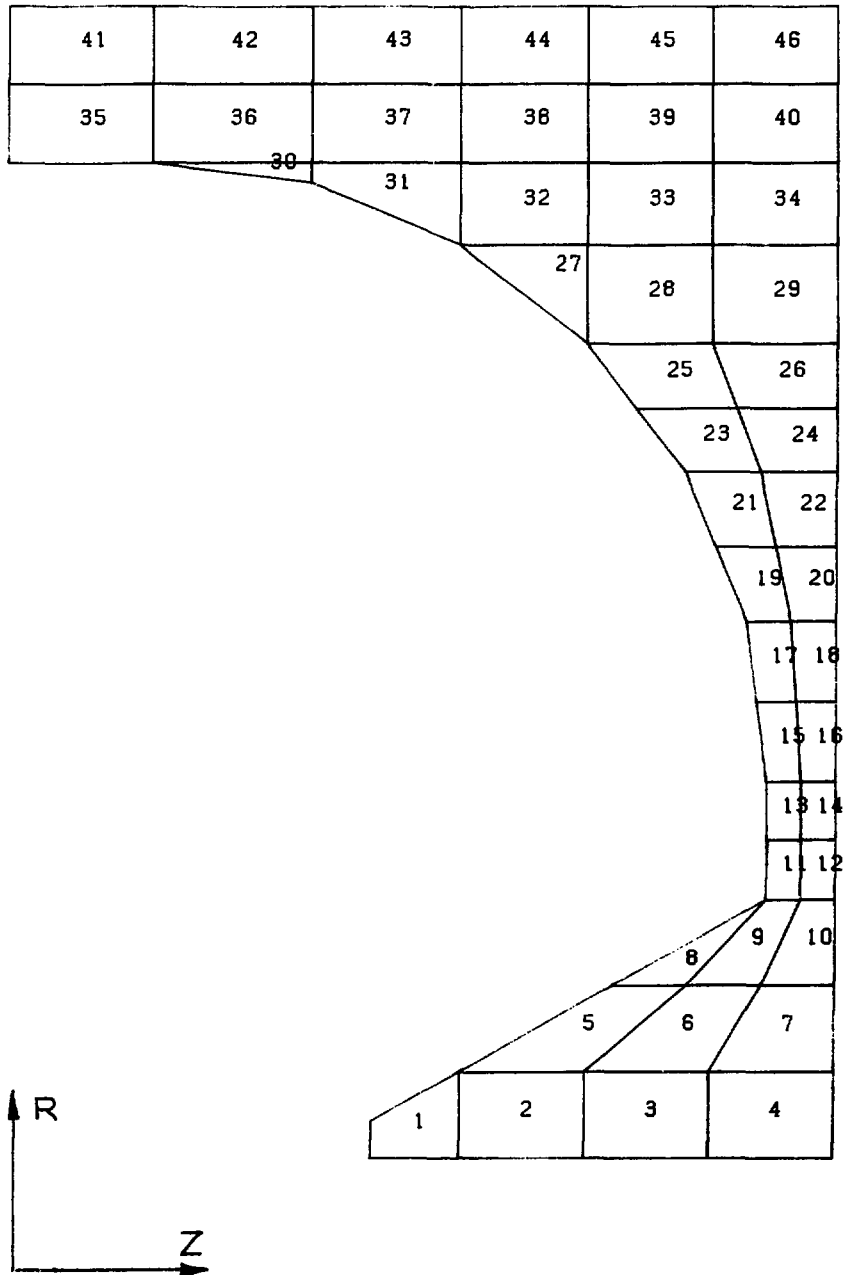
Fig. 14 Finite-element model of the 1300 MHz accelerating cavity segment.
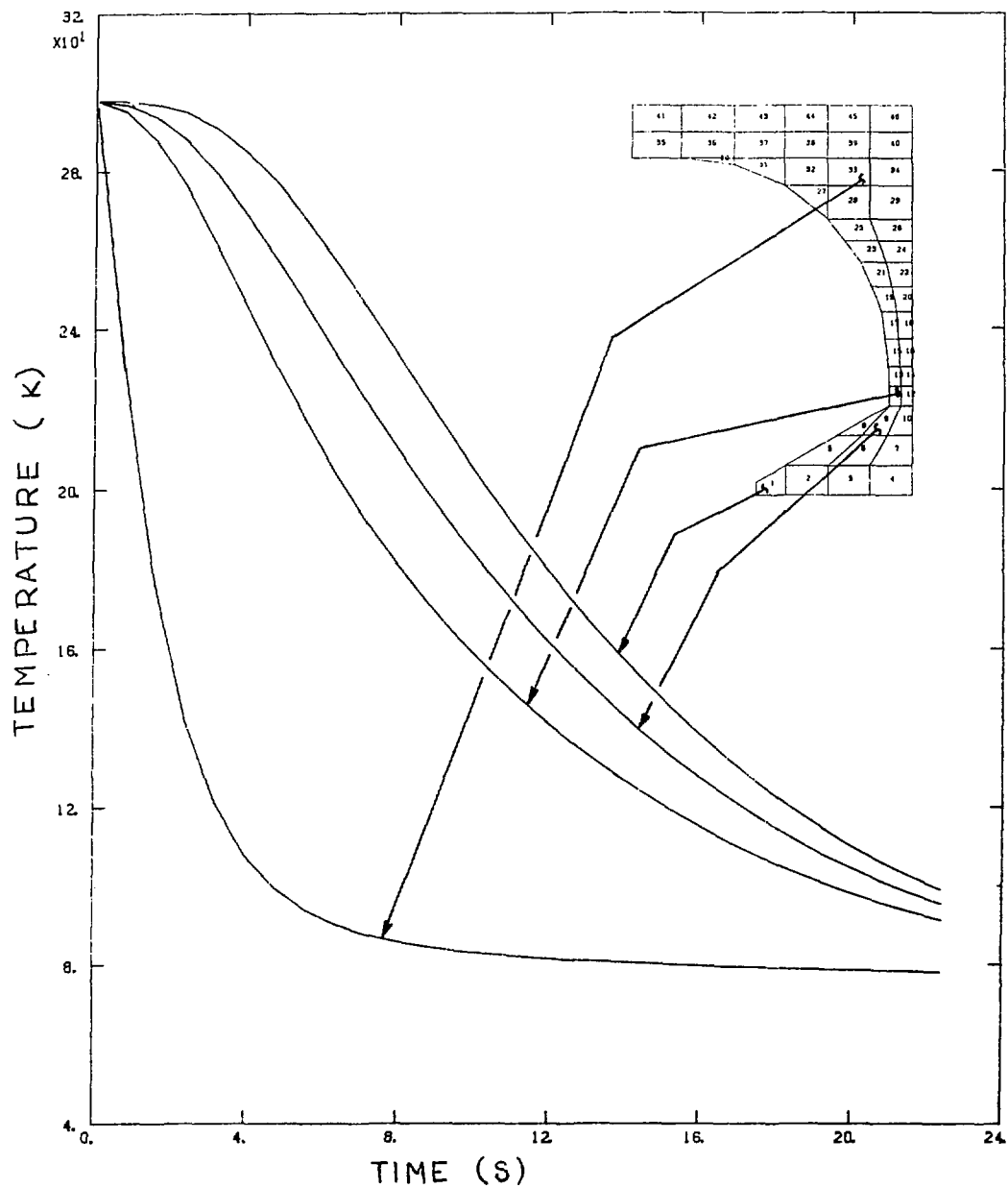
Fig. 15 Transient temperature history during cavity quenching in liquid
nitrogen (temperature in K).
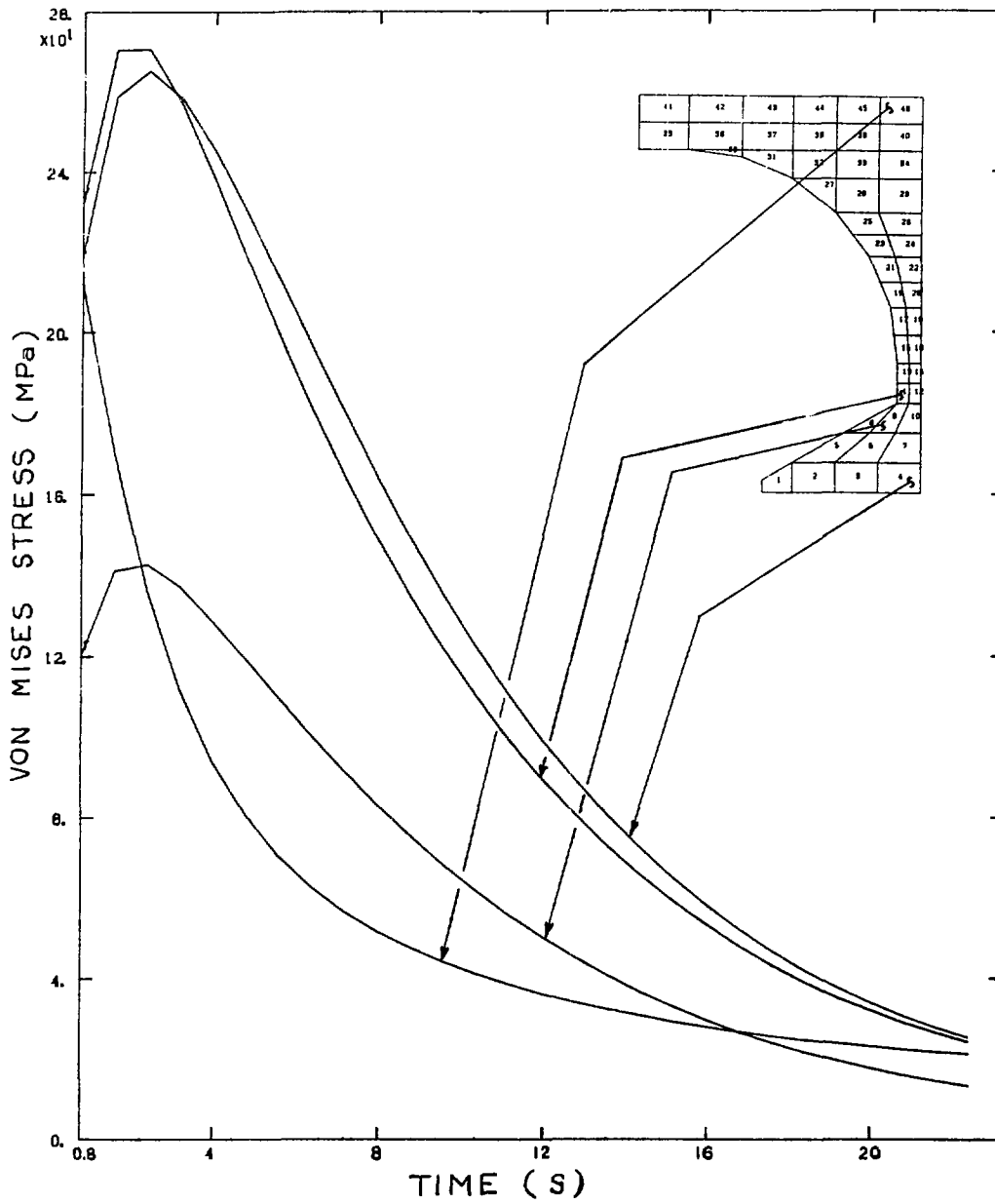
Fig. 16 Transient thermal stress history during cavity quenching in liquid
nitrogen (Von Mises stress in MPa).
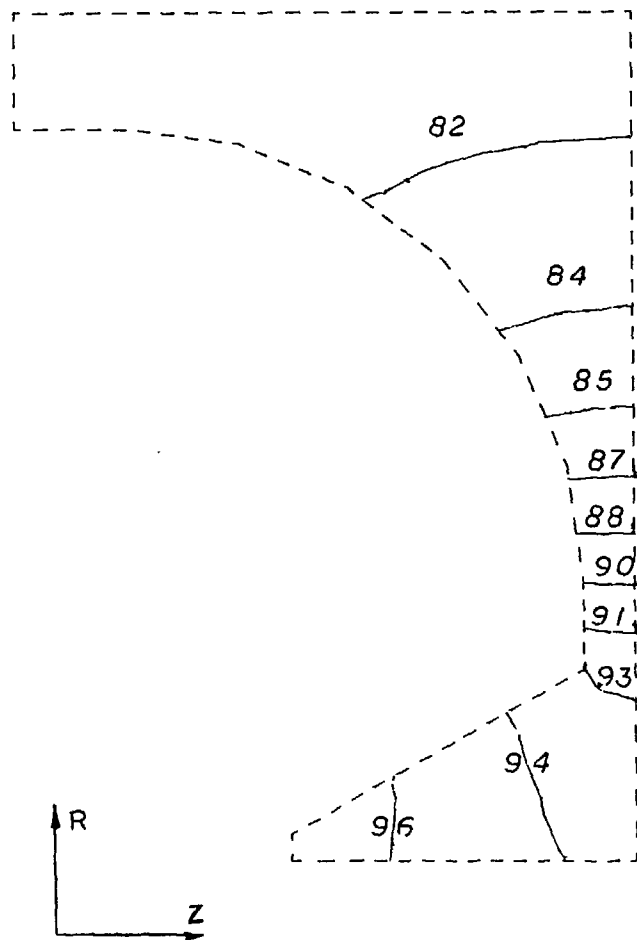
Fig. 17 Isotherms in the liquid nitrogen
cooled 1300 MHz side-coupled cavity
at a power level of 10 kW/m, (K).
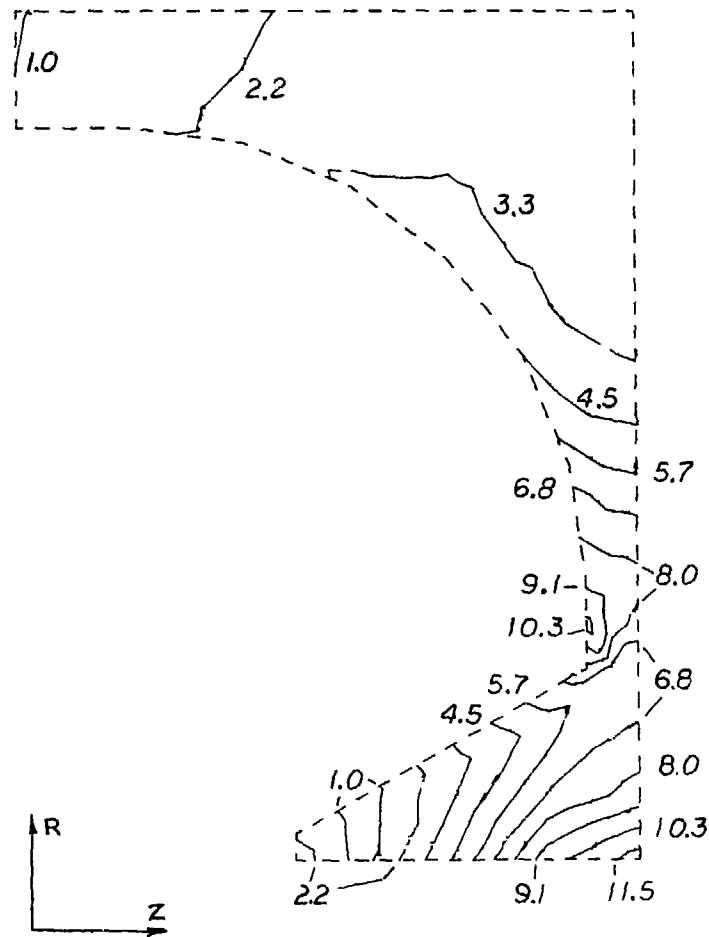
Fig. 18 Von Mises stress contours in the liquid
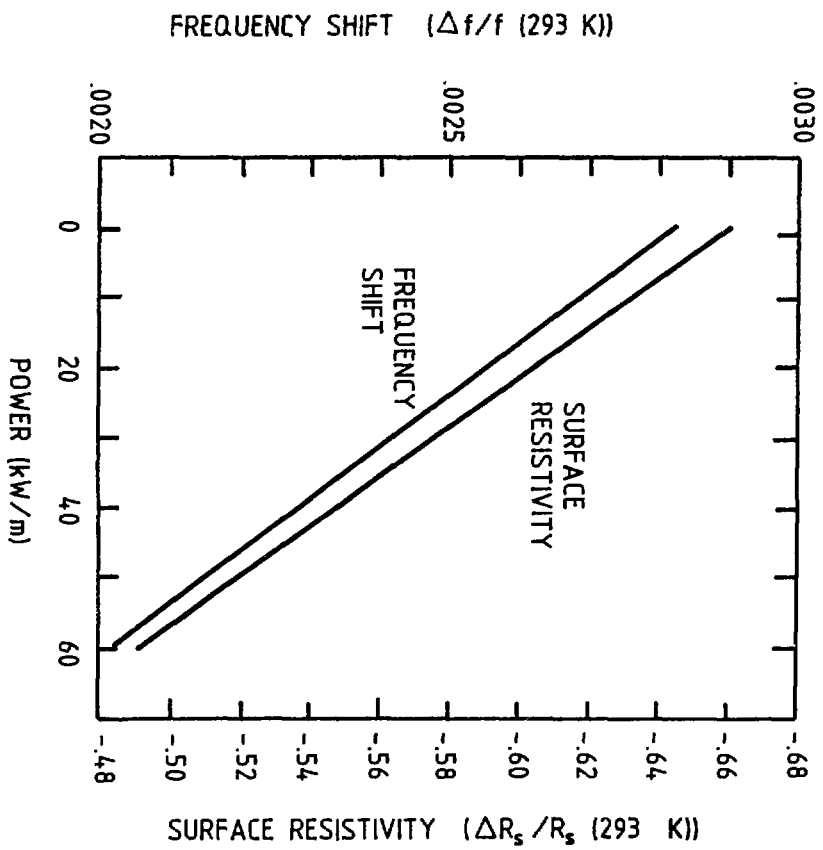nitrogen cooled 1300 MHz side-coupled
cavity at a power level of 10 kW/m, (MPa).

MAXIMUM VON MISES STRESS (MPa)

POWER LEVEL (kW/m)

FREQUENCY SHIFT ($\Delta f/f$ (293 K))
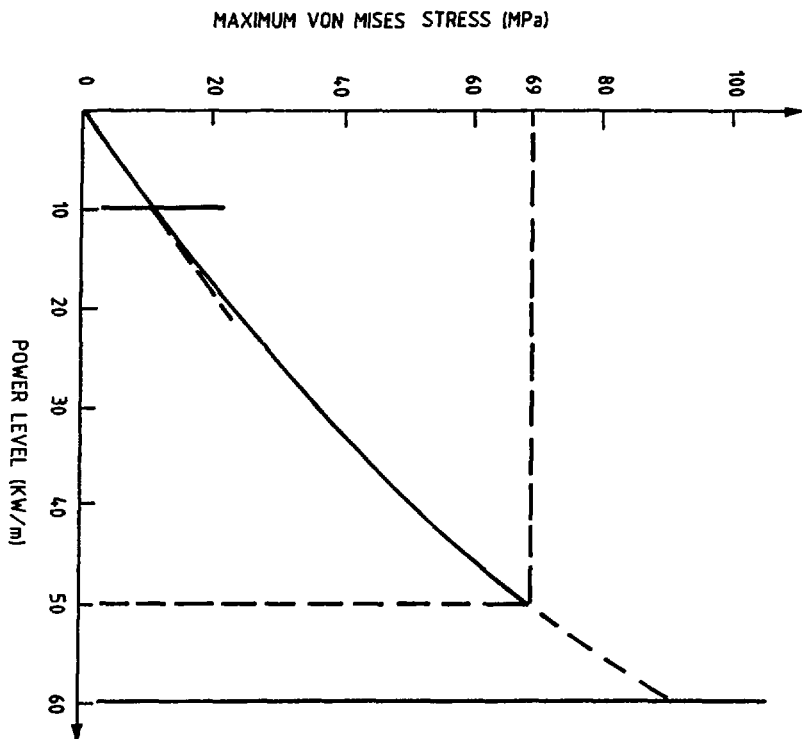
Fig. 19 Variation of the maximum Von Mises stress in the liquid nitrogen cooled 1300 MHz side-coupled cavity.

POWER (kW/m)

FREQUENCY SHIFT

SURFACE RESISTIVITY

SURFACE RESISTIVITY ($\Delta R_s/R_s$ (293 K))

Fig. 20 Frequency shifts and change in surface resistivity in the liquid nitrogen cooled 1300 MHz side-coupled structure.